Available online at www.sciencedirect.com
SCIENCE DIRECT®
Journal of the European Ceramic Society 25 (2005) 1723–1731
www.elsevier.com/locate/jeurceramsoc

Degradation of mechanical and electrical properties after long-term oxidation and corrosion of non-oxide structural ceramic composites

Valentina Medri[a], Marek Bracisiewicz[b], Kristoffer Krnel[c], Frederic Winterhalter[a], Alida Bellosi[a,*]

[a] *CNR-ISTEC, Institute of Science and Technology for Ceramics, Via Granarolo 64, 48018 Faenza, Italy*
[b] *JRC Petten, P.O. Box 2, Petten, The Netherlands*
[c] *Jozef Stefan Institute, Jamova 39, SI-1000 Ljubljana, Slovenia*

Available online 5 February 2005

Abstract

This work summarizes the results related to the influence of the starting composition and of microstructure on properties degradation, due to oxidation and corrosion, relatively to the following structural ceramics: Si_3N_4–TiN, Si_3N_4–$MoSi_2$, AlN–SiC–$MoSi_2$, AlN–SiC.The effects of: (i) long-term oxidation in air (100 h), in the temperature range 600–1500 °C and (ii) of long-term corrosion (400 h) in acid or basic aqueous solution at RT, 40 and 70 °C, on the electrical resistivity and mechanical strength of the composites are analysed and compared. The degradation of the properties are related to the characteristics of the surface and sub-surface damage after oxidation and corrosion treatments.

Keywords: Composites; Corrosion; Electrical properties; Mechanical properties; Oxidation

1. Introduction

The control of the mechanical and electrical behaviours of electroconductive structural ceramic composites is essential in order to know the limit for engineering uses. Nitrides like silicon nitride and aluminium nitride can be applied up to about 1200 °C under oxidizing atmosphere. Composites obtained with the addition of an electroconductive secondary phase such as TiN, TiB_2, TaN, TiCN, TiC, $MoSi_2$ and ZrN[1–17] can result in improved toughness and strength and high electrical conductivity, this latter property being essential for specific applications in the field of high temperature heaters, igniters and heat exchangers. However, most of these phases are easy-to-oxidize, therefore, possible damages and properties degradation derive from oxidation/corrosion environmental conditions.

It is well-known that the high temperature mechanical properties and the oxidation and corrosion behaviour of silicon nitride-, silicon carbide-, aluminium nitride-based materials and composites strongly depend on the microstructure (porosity and grain size of the secondary phase) and composition (amount of secondary phase, impurities and sintering aids). The intergranular glassy phases play a crucial role in oxidation behaviour because it provides a continuous transport medium between the bulk and the oxide scale, due to the outward diffusion of cations (such as cations deriving form the sintering aids or impurities) and inward diffusion of oxygen.[18–25]

The oxidation of electroconductive composites is also affected by the type and amount of the secondary phases, because TiN, TiB_2, $MoSi_2$ start to oxidize at relatively low temperatures (500–700 °C) compared to the matrix materials.[26] Oxidation and corrosion of non-oxide ceramic composites results in different behaviours and mechanisms depending on the temperature, besides the matrix microstructure and type and amount of the electroconductive particles.[18–25,27–32] In particular, chemical reactions leading to oxidation of silicon nitride or aluminium nitride matrices containing titanium nitride or molybdenum disilicide are accompanied by several diffusion phenomena, therefore, the complex interactions among the involved species at the reaction interface and

* Corresponding author. Tel.: +39 0546 699724; fax: +39 0546 46381.
E-mail address: bellosi@istec.cnr.it (A. Bellosi).

0955-2219/$ – see front matter © 2004 Elsevier Ltd. All rights reserved.
doi:10.1016/j.jeurceramsoc.2004.12.002

inside the growing oxide scale and the development of complex product layers affect the overall oxidation behaviour.

This paper shows the results of long-term oxidation and corrosion in aqueous basic or acid solutions on flexural strength and electrical resistivity of full dense composites in the systems: AlN–SiC, AlN–SiC–$MoSi_2$, Si_3N_4–$MoSi_2$ and Si_3N_4–TiN.

2. Experimental procedure

The ceramic composites were produced starting from the following powder mixtures (amounts in vol.%):

AlN + 21SiC	Si_3N_4 + 35TiN
AlN + 15SiC + 30$MoSi_2$	Si_3N_4 + 35$MoSi_2$

Sintering aids where also added: 2 wt.%Y_2O_2 and 2 wt.%Al_2O_3 + 5 wt.%Y_2O_3 to the AlN- and Si_3N_4-based composites, respectively.

Fully dense materials in the systems AlN–SiC and AlN–SiC–$MoSi_2$ were obtained by pressureless sintering at 1900 °C for 1 h, while the Si_3N_4-based composites were produced by hot pressing at 1800 °C, applying a pressure of 30 MPa. Details on processing and microstructure are reported in previous papers.[5,6]

For *oxidation and corrosion tests*: bend bars specimens with chamfered edges were used. The specimens were cleaned in ultrasonicated acetone bath, dried, weighed (accuracy 0.01 mg). Mass change was measured after oxidation or corrosion tests.

Oxidation tests were carried out at temperatures of 800, 1000, 1200, 1300, 1400, 1500 °C for 100 h. At least 5 bars were oxidized for each selected condition.

Corrosion tests were performed in 1.8 M sulphuric acid or 4 M sodium hydroxide aqueous solutions, at room temperature (RT, ∼20), 40 and 70 °C for 400 h.

Microstructural characteristics of the specimens before and after oxidation were analysed through X-ray diffraction and scanning electron microscopy (SEM). In particular, the exposed surfaces, the polished cross-sections and the fracture surfaces were examined.

Flexural strength (σ) on as sintered, oxidized or corroded specimens was measured using a four point bending jig with a lower span 20 mm and an upper span 10 mm on an universal screw type testing machine Zwick/Roell Z050, using a crosshead speed of 0.5 mm/min. These tests were performed at room temperature.

The electrical resistivity (ρ) was measured on the as sintered, oxidized and corroded plates at room temperature by means of four probe dc method and two probe dc method, inducing in both cases a longitudinal current along the plates. The current and voltage readings were made at the same time in two different digital high-resolution multimeters. The resistivity values were determined from the electrical resistance measurements taking into account the test leads distance and cross-section area of the samples.

On the most corroded samples volume resistivity measurements were performed with a guarded resistivity cell in conjunction with a high resistance meter. The specimens were placed in the test chamber with two conductive rubber electrodes between the sample and the metal electrodes of the cell. The measurements were carried out by applying a voltage of 25 V and waiting 2 min before reading the electrical resistance value. The resistivity values were determined from the resistance measurements taking into account the surface area of the main electrodes and the thickness of the samples.

3. Results and discussion

3.1. AlN-based composites

3.1.1. Microstructure of the pressureless sintered composites

The pressureless sintered materials are fully dense. The microstructure in Fig. 1a of the composite AlN–SiC–$MoSi_2$ evidences bright particles ($MoSi_2$), dark-phase grains (AlN and SiC) and intermediate grey contrast grain boundary

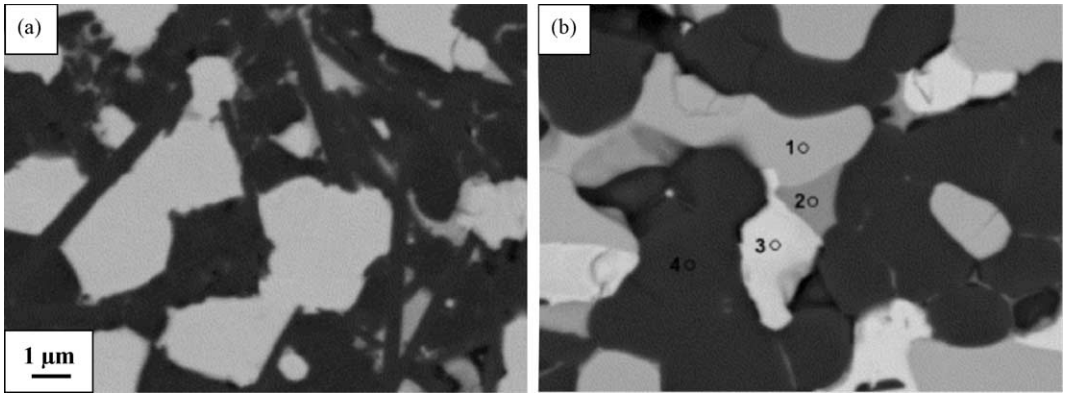

Fig. 1. Microstructure of the AlN–SiC–$MoSi_2$ composite revealed on the polished surface (a). Micrograph (b) highlights the following phases: (1) $MoSi_2$, (2) grain boundary phase YAG ($Y_3Al_5O_{12}$), (3) Mo_5Si_3 and (4) AlN–SiC.

phase, that is crystalline YAG ($Al_5Y_3O_{12}$).[6] The presence of glassy yttrium silicates cannot be excluded. There are no cracks visible between $MoSi_2$ and the matrix phase, in spite of quite different thermal expansion coefficients of the present phases, which indicates good adhesion among the grains of different composition. Some $MoSi_2$ grains (an example is shown in Fig. 1b contain areas appearing with two different grey levels that correspond to different stoichiometries. The brighter part contains a higher amount of Mo, as it is composed by phases with a stoichiometry close to Mo_5Si_3 and $Mo_{4.6}Si_3C_{0.6}$, confirming the results of XRD analyses. The EDX analyses of $MoSi_2$ grains reveal also a small amount of Al. In the sintered composite only hexagonal 2H SiC was detected and this phase can form solid solutions with hexagonal AlN, due to their matching lattice parameters. As a matter of fact, some elongated AlN grains were observed (Fig. 1a) inside, which Si was detected using EDX microanalysis. This supports the hypothesis of partial formation of solid solutions, since the elongated grains grew from liquid phase present during sintering.[6]

The microstructure of the composite AlN–SiC (Fig. 2a and b) is constituted by uniform grains with a mean grain size of the AlN–SiC phase of about 2 μm and by the presence of intergranular phase having compositions next to that of YAG phase ($Al_5Y_3O_{12}$), however, the presence of glassy yttrium silicates cannot be excluded. The crystalline phases are AlN, β-SiC and YAG. An extensive formation of AlN–SiC solid solutions can be ruled out in these samples, since β-SiC peaks are clearly visible in the XRD spectra. However, comparing the relative intensities of the main peaks of AlN and SiC, the calculation of the corresponding amount of these phases, yields 7.5 vol.% of SiC in the AlN–SiC mixture after sintering, which is considerably lower than the SiC starting amount. Moreover, the variation of the cell parameters of AlN (compared to pure AlN phase) suggest that about 10 vol.% of SiC formed solid solutions with AlN, but owing to the relatively low temperature, the formation of solid solutions was not completed. On the other hand, according to studies reported in literature,[33–36] 1900 °C as sintering temperature is a lower limit for AlN–SiC solid solution formation in the compositions range of 20–80 wt.% SiC.

Table 1
Flexural strength values in function of the oxidation temperature measured on samples oxidized for 100 h

Oxidation temperature (°C)	AlN–SiC (σ, MPa)	AlN–SiC–$MoSi_2$ (σ, MPa)
As-sintered	379 ± 58	359 ± 17
600		328 ± 35
800		361 ± 51
1000	283 ± 44	
1200	266 ± 44	373 ± 40
1300		382 ± 39
1400	88 ± 11	356 ± 15
1500		361 ± 42

The values of the as sintered materials (AlN–SiC and AlN–SiC–$MoSi_2$ composites) are reported as well.

3.1.2. Long-term oxidation and properties degradation

The long-term oxidation tests in air at temperatures between 600 and 1500 °C induce surface and subsurface modification that involve the oxidation of the phases present in the composite and the reactions among the oxidation products. Pure AlN and SiC have high oxidation resistance and develop protective oxide scales based on SiO_2 and Al_2O_3. In contrast, pure $MoSi_2$ undergoes rapid oxidation and consequent pesting at temperatures between 500 and 800 °C (due to the formation of volatile Mo-oxides),[26] while its oxidation resistance is excellent at temperatures higher than 1000 °C, due to the formation of a protective surface layer of SiO_2.[23,26]

The AlN–SiC–$MoSi_2$ composite exhibits high oxidation resistance over the whole temperature range. No pesting of $MoSi_2$ is observed during treatments in the temperature range at 500–800 °C, very likely due to Al incorporation into the $MoSi_2$ lattice.[26] In addition, the high density of the composite is a positive factor against the massive oxidation of $MoSi_2$. At high temperatures 1200–1500 °C a growing oxide scale based on mullite proves to be highly protective.[23]

The composite AlN–SiC is stable up to about 1200 °C.[24] Thereafter a porous oxide scale based on alumina and mullite form on the surface.

The fracture strength values for samples oxidized at various temperatures are reported in Table 1. The strength of non-oxidized samples AlN–SiC–$MoSi_2$ is comparable with the values measured in the AlN–SiC materials.

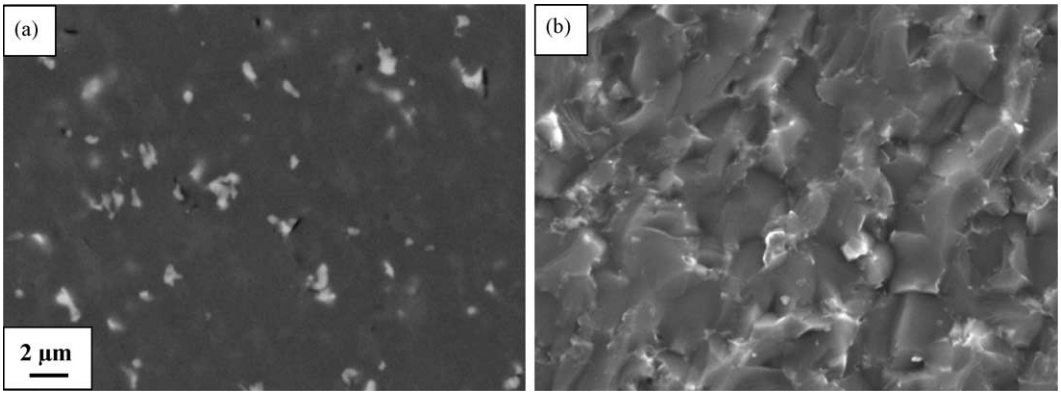

Fig. 2. Micrtostructure of the composite AlN–SiC: (a) polished surface and (b) fracture surface.

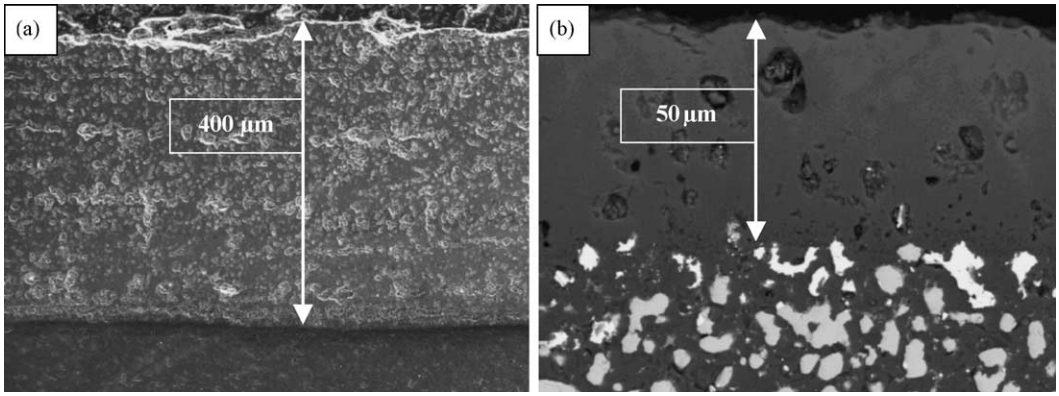

Fig. 3. Microstructure of the cross-section of samples oxidized for 100 h at 1400 °C: (a) AlN─SiC and (b) AlN─SiC─$MoSi_2$.

For the composite AlN–SiC–$MoSi_2$ the changes in strength after oxidation are small and all within the standard deviation.[22] The oxidation does not seem to have detrimental effects on this composite. A little lower strength value at 600 °C can result from evaporation of MoO_3 form the surface due to limited oxidation of $MoSi_2$. At this temperature the oxidation is not fast enough to form a protective layer of mullite, as observed in the samples oxidized at 1200–1300 °C: in this case mullite could be the reason for a little strength improvement, due to partial sealing of pre-existing surface critical defects. Oxidation at the highest temperatures (1400–1500 °C) affects the strength, which however, is still in the range of the starting material.

The strength degradation due to oxidation for the AlN–SiC composite is limited in the samples oxidized up to 1200 °C (oxidation very low), while it is strong after oxidation at 1400 °C.[24] In fact, at temperatures above 1350 °C the formation of a thick oxide scale occurs. The oxide scale is porous and formed by mullite and alumina. Fig. 3 evidences that the strength degradation behaviour in the two tested materials is related to different oxide scales. After oxidation at 1400 °C, the composite AlN–SiC (Fig. 3a) exhibits a 400 μm porous scale, while the composite AlN–SiC–$MoSi_2$, Fig. 3b, has a very thin (50 μm), rather compact, surface scale.

The electrical resistivity of the AlN–SiC–$MoSi_2$ composite increases from 10^{-3} Ω cm in the as sintered material,[6] to about 10^5 and 10^7 Ω cm after oxidation at 600 and 800 °C, respectively. This is expected on the basis of partial decomposition and volatilization of the electrically conductive phase ($MoSi_2$). In the samples treated at higher temperatures (1300–1400 °C) the resistivity approaches a value of $\sim 10^{11}$ not far from that of mullite, 10^{13} Ω cm. In fact the oxide layer developed at these temperatures is rather uniform and thick enough to mask the influence of the conductive bulk material.

3.1.3. Long-term corrosion and properties degradation

Corrosion tests on AlN–SiC and AlN–SiC–$MoSi_2$ evidenced a high stability of both the composites in sulphuric acid aqueous solution.

Therefore, long-term corrosion tests were performed only in NaOH corrosive solution for the sample AlN–SiC–$MoSi_2$. The grain boundary phases, which contain a very stable YAG phase and an amount of glassy Y–Si-oxynitrides and Y-silicates play an important role in corrosion. At RT the grain boundary glassy phases are dissolved rapidly inside the volume of composite attacked by the corrosion. The simultaneous corrosion of AlN and $MoSi_2$ is progressive with time: the attack on $MoSi_2$ particles occurs mainly at the particle boundaries. At 40 °C, in addition to the very fast dissolution of the grain boundary phases which also occurred at RT, AlN and $MoSi_2$ undergo dissolution at the same rate. On the other hand, at 70 °C AlN corrodes at a rate one order of magnitude higher than that of other phases.[31]

The selective corrosion of the various phases present in the sample is caused by leaching of Al, Si and Mo ions (with amphoteric and acid character), i.e. to the surface exchange between OH^+ and exchangeable ions present on the sample surface, where no barrier diminishes the effective contact area between reactants. Details on corrosion kinetics and related phenomenology are reported in a previous paper.[31]

At room temperature and 40 °C, the corrosive attack takes place mainly on the sample surface (as visible from the Fig. 4a and b), while at 70 °C a corroded sublayer increases up to 35 μm after 400 h, but the $MoSi_2$ particle network still ensures the percolation. In fact the electrical resistivity doesn't change, except for slight increase (from 1.6×10^{-3} to 3×10^{-3} Ω cm) after corrosion for 400 h at RT: this is probably due to the preferential leaching of $MoSi_2$ as highlighted by either the degree of dissolution or by the grooves around the $MoSi_2$ particle boundaries which can result in the lower contact between the $MoSi_2$ electroconductive particles.

3.2. Si_3N_4-based composites

3.2.1. Microstructure of the hot pressed composites

Both the composites were sintered to full density by hot pressing. The microstructure of the hot-pressed Si_3N_4–TiN material consists of a fine-grained matrix of β-Si_3N_4 grains, surrounded by a glassy grain boundary phase, and of well

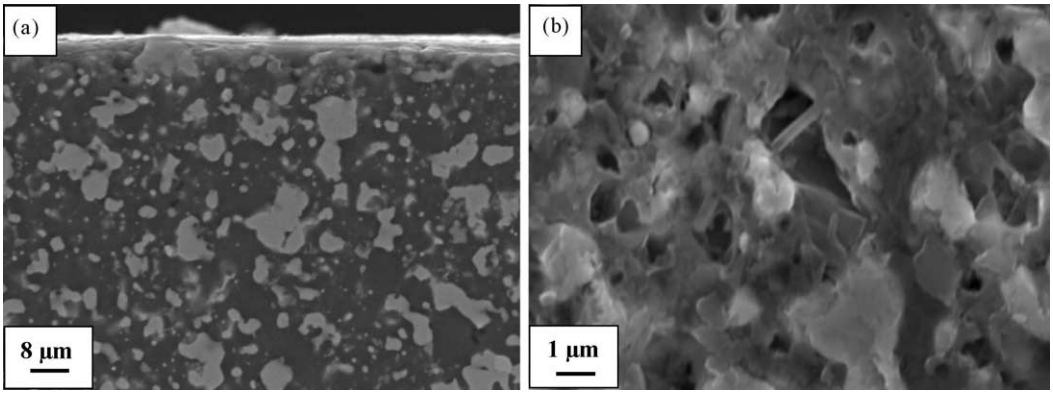

Fig. 4. Microstructure of the AlN─SiC─$MoSi_2$ composite after corrosion at 40 °C in sulphuric acid solution: (a) cross-section and (b) surface.

dispersed secondary phase (TiN) particles, Fig. 5a. The grain boundary phase is composed mainly of amorphous phases in the system Y–Al–Si–O–N; traces of yttrium titanates were revealed. The main part of alumina introduced as sintering aid enters in solid solution with β-Si_3N_4 grains during the re-precipitation phenomena that occur in the liquid-phase sintering process.

The microstructure of the hot pressed Si_3N_4–$MoSi_2$ composite consists of a fine-grained matrix of Si_3N_4 grains surrounded by a glassy grain boundary phase and of well dispersed tetragonal $MoSi_2$ particles (Fig. 5b). As crystalline phases, more than 50% of the starting α-Si_3N_4 is still present.[5] The presence of about 5 vol.% of crystalline Si_2N_2O phase is detected, favoured by the content of SiO_2 which is present either in $MoSi_2$ powder and in Si_3N_4 powder. Since no crystalline phases containing the sintering aids were revealed in the hot pressed composite, the grain boundary phases is amorphous, in the system Al–Y–Si–O–N, in a total volume of about 6%.[5] Both the composites exhibit outstanding mechanical properties.[5,21]

3.2.2. *Long-term oxidation and properties degradation*

In the oxidized samples, the strength variation (Table 2) is related to the characteristics of the surface scale and of the sub-surface damage [20,25] (examples are shown in Figs. 6 and 7): in Si_3N_4─TiN the surface scale, constituted by more or less porous TiO_2 and by silicatic phases, is less protective than the scale developed at the surface of Si_3N_4–$MoSi_2$, where a dense silica-based scale (formed at $T > \sim 1200$ °C) is well adherent to the bulk and is much thinner than the scale in the composite containing TiN.

In fact, in the composite Si_3N_4─TiN, after the treatment at 800 °C the scale is brittle, on the contrary it becomes more compact after at higher temperatures. Large cracks are present at the reaction interface in the sample treated at 1000 °C due to the thermal coefficient mismatch between the compact oxide scale and the porous sub-layer. After the treatment at 1200 °C an amount of silica embeds rutile grains and favours a good adhesion between the surface oxide scale and the sub-layer due to the penetration of silicate glass towards the bulk, partially filling the voids left by the depletion of TiN (Fig. 6a). The formation of cracks, also within the porous sub-layer, is associated with a volume expansion that accompanies the transformation of TiN to TiO_2.

The penetration of oxygen towards the bulk is influenced not only by the formation of voids left by cations diffusion and Ti depletion, but also by the protective action of viscous silicates that partly fill the voids and hinder the cracking at the oxide/sub-layer interface. In fact, the oxygen penetration is lower in the sample oxidized at 1200 °C than at 1000 °C, due to the growth of a rather compact and protective surface

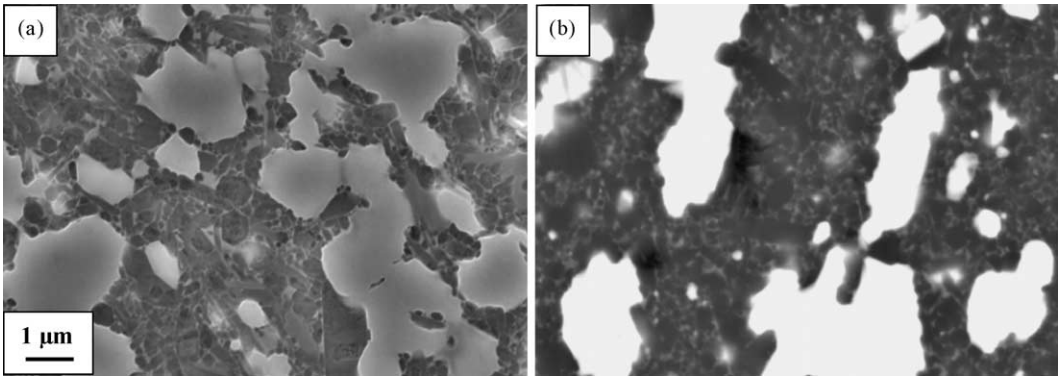

Fig. 5. Microstructure of the polished surfaces of the Si_3N_4─TiN (a) and Si_3N_4─$MoSi_2$ and (b) composites.

Table 2
Flexural strength and electrical resistivity values in function of the oxidation temperature measured on samples oxidized for 100 h

Oxidation temperature (°C)	Si_3N_4—TiN		Si_3N_4—$MoSi_2$	
	(σ, MPa)	(ρ, Ω cm)	(σ, MPa)	(ρ, Ω cm)
As-sintered	835 ± 116	6×10^{-4}	913 ± 66	1×10^{-3}
800	807 ± 68	1×10^{11}	916 ± 20	3×10^{7}
1000	671 ± 88	6×10^{12}	668 ± 61	1×10^{8}
1200	508 ± 81	1×10^{10}	791 ± 14	1×10^{8}
1300			844 ± 32	2×10^{9}
1400			882 ± 25	5×10^{8}
1500			836 ± 62	6×10^{8}

The values of the as sintered materials (Si_3N_4—TiN and Si_3N_4—$MoSi_2$ composites) are reported as well.

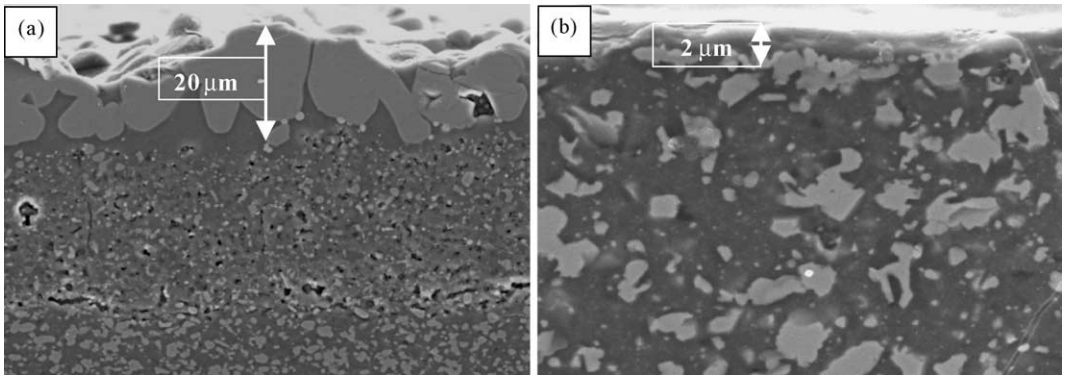

Fig. 6. Microstructure examined in the cross-section of the test samples, after oxidation at 1200 °C for 100 h: (a) Si_3N_4—TiN and (b) Si_3N_4—$MoSi_2$.

oxide scale, that is less permeable to oxygen than porous or microcracked oxide scales.

These oxidation behaviour induces a rapid strength degradation, in fact after the oxidation at 1200 °C for 100 h, the strength is more than 30% lower than in the starting material.

Instead, in the case of the composite Si_3N_4–$MoSi_2$ the oxide products formed at temperatures 1200–1500 °C are based on glassy silica, where cristobalite and Y-silicates crystallize. This scale is very protective, as highlighted also by the absence of subsurface defects after 100 h at 1400 °C (Fig. 7a) and by the very limited porosity formed after 100 h at 1500 °C (Fig. 7b).

Enhanced strength retention (Table 2) is observed for Si_3N_4–$MoSi_2$ composites oxidized over the whole range of temperatures investigated, except after oxidation at 1000 °C, that induced a strength decrease of about 25%, compared to the as-produced materials. In fact, some porosity, due to the formation of volatile Mo-oxides, is present up to a depth of 60 μm towards the bulk from the surface oxide layer.

Instead, in the temperature range 1200–1500 °C, $MoSi_2$, assisted by oxygen, reacts with Si_3N_4 forming Mo_5Si_3 and additional Si_2N_2O and SiO_2, that is the cause of the new rise of strength after the treatment at $T \geq 1200$ °C. Thus the high level of strength retention in the range temperature 1200–1500 °C is expected, because of the high volume of

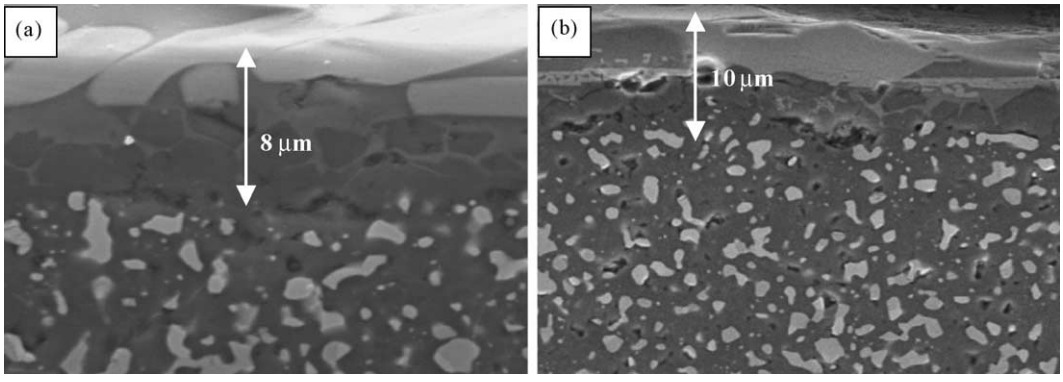

Fig. 7. Microstructure of the cross-section in the composite Si_3N_4—$MoSi_2$ after oxidation for 100 h at 1400 °C (a) and 1500 °C (b).

Table 3
Values of the flexural strength and of the electrical resistivity in function of the corrosion temperatures after 400 h in acid and basic aqueous solutions; relatively to the Si_3N_4–TiN and Si_3N_4–$MoSi_2$ composites

Corrosion temperature (°C)	Si_3N_4–TiN		Si_3N_4–$MoSi_2$			
	Acid corrosion		Acid corrosion		Basic corrosion	
	(σ, MPa)	(ρ, Ω cm)	(σ, MPa)	(ρ, Ω cm)	(σ, MPa)	(ρ, Ω cm)
RT	848 ± 69	$5–7 \times 10^{-4}$		2×10^{-3}		2×10^{6}
40	759 ± 27	$2–6 \times 10^{2}$		2×10^{-3}		5×10^{6}
70	597 ± 24	$0.6–5 \times 10^{8}$	720 ± 40	1.5×10^{5}	791 ± 29	2×10^{8}

$MoSi_2$ phase (35 vol.%): as reported by Klemm et al.,[29] increasing the amount of $MoSi_2$ in the Si_3N_4–$MoSi_2$ composites the residual strength increases after oxidation. The factor strengthening the oxidized materials is the formation, beneath the oxide scale, of a layer of Si_2N_2O: the amount of silicon oxinitride increases with temperature and prevents the damage of the bulk material, as previously observed by Klemm et al.[27–29] In fact, the present results show that the flexural strength of the oxidized specimens increases with the increase of the oxidation temperature. Otherwise, the presence of some porosity in the sub-oxide layer is due to the conversion $MoSi_2 \rightarrow Mo_5Si_3$, as the silicide particles contract their volume: the high conversion occurring at 1500 °C leads to high porosity, that counterbalances the positive effect of the oxynitrides, decreasing the strength again. It is why the higher level of strength retention is reached at 1400 °C. In any case, both at 1400 and 1500 °C (Fig. 7) the surface oxide scales did not influence the strength because they are not well adherent to the material; this is a further confirmation that the new decrease of strength at 1500 °C is due to sub-surface defects such as pores.

The electrical resistivity, that is about 10^{-3} Ω cm in both the as sintered Si_3N_4-based composites,[5,25] increases to values in the range 10^{7}–10^{13} Ω cm after oxidation (Table 2), because the surface oxide products are insulators. Electrical resistivity depends on the thickness of the oxide scale and on the adhesion of the scale to the bulk material. In the case of the composite Si_3N_4–TiN, the bulk electrical resistivity is only slightly altered by the modifications occurring during the long oxidation period (e.g. grain boundary recrystallization or formation of oxidation product) and the values ranging from about 6×10^{-4} to 1.2×10^{-3} Ω cm were measured in the samples oxidised 100 h in the temperature range 800–1200 °C.[20]

3.2.3. Long-term corrosion and properties degradation

In both the composites, the corrosion kinetics are linear indicating chemical reactions as rate controlling phenomena.[30,32] The chemical attack in sulphuric acid solution at RT and at 40 °C involves only the progressive chemical dissolution of grain boundary phases. The attack on TiN and on $MoSi_2$ occurs only at 70 °C and is more enhanced for TiN. Si_3N_4 is not or very low affected by the selected corrosive environment.[27,29] The tests on Si_3N_4–$MoSi_2$ under basic environment, i.e. NaOH aqueous solution, indicate a strong chemical dissolution of molybdenum disilicide particles (Fig. 8). Leaching of grain boundary phases occur as well, mainly due to the presence of Al (with amphoteric character) in these glassy phases.

The strength values after 400 h of exposure to acid solution (both the composites) and basic solution (composite containing molybdenum disilicide) at different temperatures are reported in Table 3.[30,32] After corrosion in acidic environment the failing of the Si_3N_4–35 vol.% $MoSi_2$ composite (the strength is about 79% of the as-sintered value) is due to the presence of the porous and thick subsurface layer affected by corrosion, while after the tests in NaOH the strength degradation (87% of the as-sintered value) is due to the increased surface population of defects caused by the leaching of the superficial $MoSi_2$ particles.

The electrical resistivity after corrosion (Table 3) is[30,32] in agreement with the observed phenomena: after the treatment at room temperature in acid solution both the composites maintain an electrical resistivity of about 10^{-3} Ω cm. After the corrosion at 40 °C: Si_3N_4–$MoSi_2$ is still a rather good electrical conductor, while Si_3N_4–TiN has a very low electrical conductivity. After the corrosion at 70 °C: both the composites can be considered electrical insulators, due to the dissolution of the electroconductive particles at the sample surface.

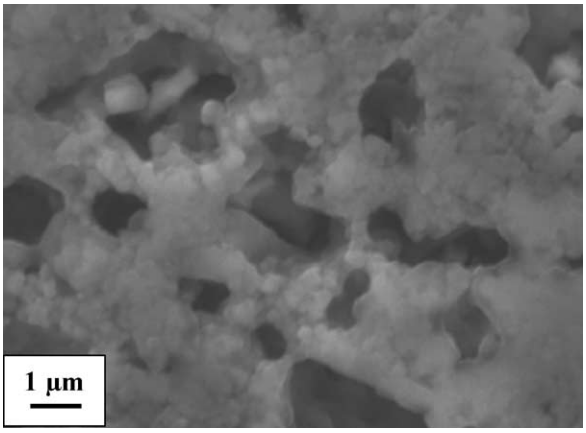

Fig. 8. Surface of the composite Si_3N_4–$MoSi_2$ after corrosion in the basic NaOH aqueous solution. $MoSi_2$ particles are completely dissolved. Grain boundary phase was leached as well.

Consequently, the long-term permanence in basic environments, the electrical resistivity of Si_3N_4–$MoSi_2$ composite improves up to 10 order of magnitude as a consequence of the corrosive attack on $MoSi_2$.[30] The progressive leak of percolation of the electroconductive particles network leaves on the surface a porous dielectric Si_3N_4, which insulates the electroconductive bulk material.

4. Conclusion

Compositing nitride ceramics (Si_3N_4, AlN) with properly selected electroconductive particulates offers great potentialities to improve mechanical properties, to obtain electroconductive reinforced ceramics and to reduce strength degradation under oxidizing atmosphere. Top application temperatures can be raised compared to those suitable for monolithic nitrides:

- for applications in the temperature range 1200–1500 °C composites Si_3N_4–$MoSi_2$ and AlN–SiC–$MoSi_2$ are preferable, they withstand long-term permanence at 1500 °C maintaining elevated strength values, with limited surface damage;
- for applications up to 1200 °C composites Si_3N_4–TiN are preferable.

Pesting of $MoSi_2$ can be avoided also in the case of applications at intermediate temperatures (500–1000 °C).

All oxidized sample evidence a strong increase of the electrical resistivity due to the external oxide scale characteristics. Bulk electrical resistivity of the oxidised Si_3N_4–TiN composite is similar to that of the as-sintered material.

These composites are also corrosion resistant:

- no acid attack on AlN–SiC–$MoSi_2$ and limited damage in basic solutions: strength and electrical resistivity values are maintained.
- limited damage in strength and electrical conductivity for acid and basic attack up to 40 °C on Si_3N_4-based composites. However, evident degradation occurs during corrosion at 70 °C.

Acknowledgements

This work was supported by the European Project R.T.N. HPRN-CT-2000-00044 “Composite Corrosion”. The authors wish to thank C. Melandri for the measurement of mechanical properties, A. Ruffini for the chemical analyses, D. Sciti and S. Guicciardi for their collaboration.

References

1. Gogotsi, Y. G., Review-particulate silicon nitride composite. *J. Mater. Sci.*, 1994, **29**, 2541–2556.
2. Huang, J.-L., Chen, S.-Y. and Lee, M.-T., Microstructure, chemical aspects and mechanical properties of TiB_2/Si_3N_4 and TiN/Si_3N_4 composites. *J. Mater. Res.*, 1994, **9**, 2349–2353.
3. Huang, J.-L., Lee, M.-T., Lu, H.-H. and Lii, D.-F., Microstructure, fracture behaviour and mechanical properties of TiN/Si_3N_4 composites. *Mater. Chem. Phys.*, 1996, **45**, 203–210.
4. Bellosi, A., Guicciardi, S. and Tampieri, A., Development and characterization of electroconductive Si_3N_4–TiN composites. *J. Eur. Ceram. Soc.*, 1992, **9**, 82–93.
5. Sciti, D., Guicciardi, S. and Bellosi, A., Microstructure and properties of Si_3N_4–$MoSi_2$ composite. *J. Ceram. Proc. Res.*, 2002, **3**, 87–95.
6. Sciti, D., Guicciardi, S., Melandri, C. and Bellosi, A., High-temperature resistant composite in the AlN–SiC–$MoSi_2$ system. *J. Am. Ceram. Soc.*, 2003, **86**, 1720–1726.
7. Petrovic, J. J., Pena, M. I. and Kung, H., Fabrication and microstructure of $MoSi_2$-reinforced Si_3N_4. *J. Am. Ceram. Soc.*, 1997, **80**, 1111–1116.
8. Huang, J.-L. and Jih, J.-M., Investigation of SiC–AlN: Part II. Mechanical properties. *J. Am. Ceram. Soc.*, 1996, **79**(5), 1262–1264.
9. Kao, M.-Y., Properties of silicon nitride–molybdenum disilicide particulate ceramic composites. *J. Am. Cerem. Soc.*, 1993, **76**, 2879–2883.
10. Lubis, A. H., Hecht, N. L. and Graves Jr., G. A., Microstructure–property relations of hot pressed silicon carbide–aluminum nitride compositions at room and elevated temperatures. *J. Am. Ceram. Soc.*, 1999, **82**, 2481–2489.
11. Nordberg, L. O. and Ekström, T., Hot pressed $MoSi_2$-particulate reinforced α-SiAlON composites. *J. Am. Ceram. Soc.*, 1995, **78**, 797–800.
12. Nagaoka, T., Yasuoka, M., Hirao, K. and Kanzaki, S., Effects of TiN particle size on mechanical properties of Si_3N_4–TiN particulate composites. *J. Ceram. Soc. Jpn.*, 1992, **100**, 617–620.
13. Zivkovic, L. M., Boskovic, S. M. and Miljkovic, S., Sintering behaviour and microstructure development in electroconductive Si_3N_4–TiN composites. In *Advanced Science and Technology of Sintering*, ed. Stojanovic B. D. *et al.* Kluwer Academic/Plenum Publishers, New York, 1999, pp. 475–481.
14. Akimune, Y., Munakata, F., Hirosaki, N. and Okamoto, Y., Optimization of mechanical and electrical properties of TiN/Si_3N_4 material by agglomerates-microstructure control. *J. Ceram. Soc. Jpn.*, 1998, **106**, 77–80.
15. Petrovsky, V. Y. and Rak, Z. S., Densification, microstructure and properties of electroconductive Si_3N_4–TaN Composites. Part I: Densification and microstructure. *J. Eur. Ceram. Soc.*, 2001, **21**, 219–235.
16. Petrovsky, V. Y. and Rak, Z. S., Densification, microstructure and properties of electroconductive Si_3N_4–TaN Composites. Part II: Electrical and mechanical properties. *J. Eur. Ceram. Soc.*, 2001, **21**, 237–244.
17. Herrmann, H., Balzer, B., Schubert, C. and Hermel, W., Densification, microstructure and properties of Si_3N_4–TiCN composites. *J. Eur. Ceram. Soc.*, 1993, **12**, 287–296.
18. Klein, R., Medri, V., Desmaison Brut, M., Bellosi, A. and Desmaison, J., Influence of additive content on the high temperature oxidation of silicon nitride-based composites. *J. Eur. Ceram. Soc.*, 2003, **23**, 603–611.
19. Mizutani, T. and Tsuge, A., Effects of metallic boride dispersion on fracture toughness and oxidation resistance in SiC ceramics. *J. Ceram. Soc. Jpn. Int. Ed.*, 1992, **100**, 979–982.
20. Bracisiewicz, M., Medri, V. and Bellosi, A., Factors inducing degradation of properties after long term oxidation of Si_3N_4–TiN composites. *Appl. Surf. Sci.*, 2002, **202**, 139–149.
21. Guicciardi, S., Melandri, C., Medri, V. and Bellosi, A., Effect of thermal treatments on properties of a Si_3N_4–TiN composite. *Mater. Sci. Eng. A*, 2003, **360**, 35–45.
22. Krnel, K., Sciti, D. and Bellosi, A., Influence of long term oxidation on microstructure and properties of AlN–SiC–$MoSi_2$ composite. *J. Eur. Ceram. Soc.*, 2003, **23**, 3135–3146.

23. Krnel, K., Sciti, D. and Bellosi, A., Surface modifications and oxidation kinetics of hot-pressed AlN—SiC—$MoSi_2$ electroconductive ceramic composite. *Appl. Surf. Sci.*, 2003, **210**, 274–285.
24. Sciti, D., Winterhalter, F. and Bellosi, A., Oxidation behaviour of a pressureless sintered AlN—SiC composite, *J. Mater. Sci.*, 2004, **39** 6965–6973.
25. Medri, V. and Bellosi, A., Factors inducing degradation of properties after long term oxidation of Si_3N_4—$MoSi_2$ electroconductive composites. *J. Mater. Res.*, 2004, **19**, 1567–1574.
26. Maruyama, T. and Yanagihara, K., High temperature oxidation and pesting of $Mo(Si,Al)_2$. *Mater. Sci. Eng. A*, 1997, **239/240**, 828–841.
27. Klemm, H., Taut, C. and Wötting, G., Long-term stability of nonoxide ceramics in an oxidative environment at 1500 °C. *J. Eur. Ceram. Soc.*, 2003, **23**, 619–627.
28. Klemm, H. and Schubert, C., Silicon nitride/molybdenum disilicide composite with superior long-term oxidation resistance at 1500 °C. *J. Am. Ceram. Soc.*, 2001, **84**, 2430–2432.
29. Klemm, H., Tangermann, K., Schubert, C. and Hermel, W., Influence of molybdenum silicide additions on high-temperature oxidation resistance of silicon nitride materials. *J. Am. Ceram. Soc.*, 1996, **79**, 2429–2435.
30. Winterhalter, F., Medri, V., Ruffini, A. and Bellosi, A., Corrosion of Si_3N_4—$MoSi_2$ ceramic composite in acid and basic aqueous environments: surface modifications and properties degradation. *Appl. Surf. Sci.*, 2004, **225**, 100–115.
31. Krnel, K., Medri, V., Ruffini, A. and Bellosi, A., Corrosion of electroconductuiveAlN—SiC—$MoSi_2$ ceramic composite in sodium hydroxide aqueous solution. *Corrosion*, 2003, **59**, 765–773.
32. Bracisievicz, M., Medri, V., Ruffini, A. and Bellosi, A., Corrosion of hot pressed Si_3N_4—TiN composite in sulphuric acid aqueous solutions. *Corrs. Sci.*, 2003, **45**, 2525–2539.
33. Huang, J.-L. and Jih, J.-M., Investigation of SiC—AlN system: Part I. Microstructure and solid solution. *J. Mater. Res.*, 1995, **10**, 651–658.
34. Rafaniello, W., Plichta, M. R. and Virkar, A. V., Investigation of phase stability in the system SiC—AlN. *J. Am. Ceram. Soc.*, 1993, **66**, 272–275.
35. Li, J.-F., Kawasaki, A. and Watanabe, R., Hot isostatically pressed SiC—AlN powder mixtures: effect of milling on solid solution formation and related properties. *J. Am. Ceram. Soc.*, 1998, **81**, 1445–1452.
36. Li, J.-F. and Watanabe, R., Preparation and mechanical properties of SiC—AlN ceramic alloy. *J. Mater. Sci.*, 1991, **26**, 4813–4817.